Journal of Alloys and Compounds 886 (2021) 161278

Contents lists available at ScienceDirect

Journal of Alloys and Compounds

journal homepage: www.elsevier.com/locate/jalcom

Effects of LiF on crystal structure, cation distributions and microwave dielectric properties of $MgAl_2O_4$

Tianying Qin[a,b], Chaowei Zhong[a,b,*], Yong Shang[a,c], Lei Cao[a,b], Mingxia Wang[a,b], Bin Tang[a,b], Shuren Zhang[a,b]

[a] School of Electronic Science and Engineering, University of Electronic Science and Technology of China, Chengdu 610054, China
[b] Key Laboratory of Multi-Spectral Absorbing Materials and Structures of Ministry of Education, University of Electronic Science and Technology of China, China
[c] China Zhenhua Group Yunke Electronic Co., LTD, China

ARTICLE INFO

Article history:
Received 8 March 2021
Received in revised form 20 July 2021
Accepted 21 July 2021
Available online 26 July 2021

Keywords:
$MgAl_2O_4$
Nuclear magnetic resonance
Cation distribution
Microwave dielectric properties

ABSTRACT

In this work, $MgAl_2O_4$ + xLiF (x = 0, 3.2, 6.4 mol. %) ceramics were synthesized by solid-state reaction method. The phase information of a spinel structure was delineated by XRD. The crystal structure of $MgAl_2O_4$ + xLiF (x = 0, 3.2, 6.4 mol. %) ceramics were discussed with the help of Rietveld refinements. As x increased from 0 to 6.4 mol. %, the tetrahedral sites in $MgAl_2O_4$ ceramics gradually were occupied by Al^{3+} cations, which is confirmed by ^{27}Al NMR and Raman spectra. Such the occupation of Al^{3+} cations increased the covalency (f_c/s) value of M-O (M = Mg, Al) bond in MO_4 tetrahedral of $MgAl_2O_4$ + xLiF (x = 0, 3.2, 6.4 mol. %) ceramics. LiF is mainly used as a sintering aid to improve the formation of the $MgAl_2O_4$ ceramics. In order to obtain high $Q\times f$ value spinel ceramics, LiF must be removed before the final stage of densification. In addition, the dielectric constant (ε_r), grain size and quality factor ($Q\times f$) value are significantly affected by the LiF content. However, the temperature coefficient of resonance frequency (TCf) values were independent of LiF content. $MgAl_2O_4$ + xLiF (x = 0, 3.2, 6.4 mol. %) ceramics with x = 6.4 has excellent microwave dielectric properties when sintered at 1575 °C for 8 h: ε_r = 8.36, $Q\times f$ = 99,900 GHz, TCf = − 61.57 ppm/°C.

© 2021 Elsevier B.V. All rights reserved.

1. Introduction

Due to the rapid development of high-frequency communication systems, microwave dielectric ceramic materials require low dielectric constant to reduce the signal propagation delay, high quality factor value to suppress signal attenuation, and near-zero temperature coefficient of resonance frequency to allow component to operate normally under a wide temperature range [1–5]. $MgAl_2O_4$ microwave dielectric ceramics have been extensively investigated due to their low dielectric constant and high quality factor value. K.P. Surendran et al. reported the ε_r, $Q\times f$ and TCf values of $MgAl_2O_4$ ceramics are 7.9, 68,900 GHz and − 75 ppm/℃, respectively [6]. $MgAl_2O_4$ is reported to have an intermediate spinel structure, and the general molecular formula is $(Mg_{1-\lambda}Al_{\lambda})[Mg_{\lambda}Al_{2-\lambda}]O_4$, which λ is refers to the degree of inversion [7–9]. E. S. (Merijn) Blaakmeer et al. used ^{27}Al nuclear magnetic resonance (NMR) to study the λ value of Lithium-doped $MgAl_2O_4$ [10]. Moreover, S. Takahashi et al. reported that Al^{3+} cations preferentially occupying tetrahedral sites of $MgAl_2O_4$ ceramics, which can improve the $Q\times f$ value of $MgAl_2O_4$ ceramics [11]. According to previous research results, we can use NMR data to obtain the preferential positions of Al^{3+} cations to discuss the change of $Q\times f$ value of $MgAl_2O_4$ ceramics.

LiF has been proven to be a suitable additive to significantly improve the formation of the $MgAl_2O_4$ ceramics. LiF melts at 840 °C and the addition of LiF will form a transient liquid phase around the spinel phase to promote particle rearrangement. The chemical reaction between LiF and $MgAl_2O_4$ during the sintering process can be described as below [12–15]:

$$3LiF(l) + MgAl_2O_4(s) \rightarrow LiF{:}\ MgF_2 + 2LiAlO_2 \quad (1)$$

Where (l) stands for liquid, and (s) stands for solid phase. With the increase of temperature, and the following reaction occurs:

$$LiF{:}\ MgF(l) \rightarrow LiF(g) + MgF_2(g) \quad (2)$$

Where (g) stands for gas phase. Then the highly active MgF_2 will react with $LiAlO_2$ as newly formed LiF evaporates, accompanied by the reformation of spinel:

$$MgF_2 + 2LiAlO_2 \rightarrow 2LiF(g) + MgAl_2O_4(s) \quad (3)$$

* Corresponding author at: School of Electronic Science and Engineering, University of Electronic Science and Technology of China, Chengdu 610054, China.
E-mail address: chaoweizhong1502@gmail.com (C. Zhong).

https://doi.org/10.1016/j.jallcom.2021.161278
0925-8388/© 2021 Elsevier B.V. All rights reserved.

At high temperature, LiF will evaporate from $MgAl_2O_4$ ceramics. Controlling the content of LiF, dense pure $MgAl_2O_4$ ceramics can be obtained. This phenomenon has been confirmed. Such as I. E. Reimanis et al. reported that $MgAl_2O_4$ doped with small amount of LiF sintered at 1550 ℃, Li and F ions will diffuse out of the spinel lattice [16]. This process eventually leads to the formation of dense pure $MgAl_2O_4$ ceramic. The sintering reaction of LiF-doped $MgAl_2O_4$ ceramics and the relationship between LiF and the optical properties of $MgAl_2O_4$ ceramics have been reported [14,16]. However, the effect of LiF on the microwave dielectric properties of $MgAl_2O_4$ ceramics remains unclear. Therefore, in this paper, the $MgAl_2O_4$ + xLiF (x = 0, 3.2, 6.4 mol. %) ceramics were synthesized by conventional solid-state reaction method, and the influence of LiF on the cation distributions and microwave dielectric properties of $MgAl_2O_4$ ceramics was systematically investigated.

2. Experimental method

The raw powders of MgO (>99%) and Al_2O_3 (> 99%) were weighed according to $MgAl_2O_4$ chemical formula and ball-milled with ethanol for 6 h. Subsequently, the mixtures were pre-sintered at 1350 ℃ for 4 h. In addition, LiF (> 99%) with different amounts (x = 0, 3.2, 6.4 mol. %) were added to the pre-sintered powder and ball-milled with ethanol for 6 h again. After that, the mixtures were added with PVA to form pellets. Finally, the prepared specimens were sintered at 1575 ℃ for 8 h in air.

The crystal phase of the specimen was analyzed by X-ray diffraction (Rigaku Industrial Corporation, Japan) with Cu Kα radiation in the 2θ range of 10–120°, with step size of 0.013°. The crystal structure was refined using GSAS-EXPGUI program. A Bruker Avance NEO 600 MHz spectrometer operating at 12 kHz was used to obtain ^{27}Al magic angle spinning NMR spectra at room temperature. The Raman spectra were acquired using a Raman microscope (LabRAM HR Evolution) at room temperature, where the 532 nm line of a constant power Ar laser source was used the excitation wavelength. The surface microstructures of $MgAl_2O_4$ + xLiF (x = 0, 3.2, 6.4 mol. %) ceramics were investigated using scanning electron microscopy (SEM, FEI Inspect F, United Kingdom). The impedance spectroscopy (IS) of $MgAl_2O_4$ + xLiF (x = 0, 3.2, 6.4 mol. %) ceramics was obtained with an impedance analyzer (SI 1260; Solartron Analytical, Farnborough, United Kingdom) in the frequency range of 100 Hz to 10 MHz. The microwave dielectric properties of $MgAl_2O_4$ + xLiF (x = 0, 3.2, 6.4 mol. %) ceramics were measured by the Hakki and Coleman method in the TE011 mode using a microwave network analyzer (HP83752A, the United States). The temperature coefficient of resonance frequency (TCf) value of $MgAl_2O_4$ + xLiF (x = 0, 3.2, 6.4 mol. %) ceramics were measured based on the difference of resonant frequency between 25 and 85 °C.

3. Results and discussion

Fig. 1 shows the XRD profiles of $MgAl_2O_4$ + xLiF (x = 0, 3.2, 6.4 mol. %) ceramics sintered at 1575 ℃ for 8 h. Regardless of the value of x, the main phase observed is $MgAl_2O_4$ (PDF#77-0435). At 2θ ≈ 49°, the prepared $MgAl_2O_4$ has one less peak compared with the standard PDF. No diffraction peaks corresponding to the second phase were observed in the entire composition range, and no phase containing Li^+ ions and F^- ions were found. Ivar E. Reimanis et al. reported the sintering reactions of LiF doped $MgAl_2O_4$ ceramics [16]. When the sintering temperature is less than 1050 ℃, LiF begins to melt, and densification occurs through the rearrangement of the starting powder particles in the liquid. With further increasing sintering temperature (>1050 ℃), LiF begins to leave the system, and this process eventually leads to the formation of pure $MgAl_2O_4$ spinel. Therefore, the phases containing Li^+ ions and F^- ions are not observed in. Furthermore, the outward diffusion of LiF will produce a surface areas of enhanced diffusion along the grain boundaries promoting grain growth. The full width at half maximum (FWHM) values of $MgAl_2O_4$ + xLiF (x = 0, 3.2, 6.4 mol. %) ceramics on (311) plane were listed in Table 1. It can be seen from Table 1 that the FWHM decreases with the increase of LiF content. A smaller FWHM value corresponds to a higher crystallinity and a larger grain size. In addition, as shown in Fig. 1, as the content of LiF increases, the diffraction peak of $MgAl_2O_4$ + xLiF (x = 0, 3.2, 6.4 mol. %) ceramics shifts to a higher 2θ, which indicates that the lattice constant of the sample is continuously decreasing.

Fig. 2 shows the ^{27}Al NMR spectra of $MgAl_2O_4$ + xLiF (x = 0, 3.2, 6.4 mol. %) ceramics sintered at 1575 ℃ for 8 h. $MgAl_2O_4$ + xLiF (x = 0, 3.2, 6.4 mol. %) ceramics generated two signals, about 10 and 70 ppm respectively [17–19]. The signal at 70 ppm is attributed to the tetrahedral coordination of Al, and the signal at 10 ppm is assigned to octahedral coordination of Al. These spectra imply that with the increase of x value, the peak intensity at about 70 ppm is gradually enhanced, while the peak intensity at 10 ppm is gradually decreased. The results show that the tetrahedron position in $MgAl_2O_4$ + xLiF (x = 0, 3.2, 6.4 mol. %) ceramics will be preferentially occupied by Al^{3+} cations with the increase of LiF content. For the sake of determination the fraction of Al^{3+} cations in the octahedral and tetrahedral positions of $MgAl_2O_4$ + xLiF (x = 0, 3.2, 6.4 mol. %) ceramics, the degree of inversion λ was calculated according to NMR data by Eq. (4) [11,20]:

$$\frac{I(AlO_4)}{I(AlO_6)} = \frac{\lambda}{2-\lambda} \tag{4}$$

Where I (AlO_4) represent the peak intensity of tetrahedrally coordinated aluminum, I (AlO_6) represent the peak intensity of

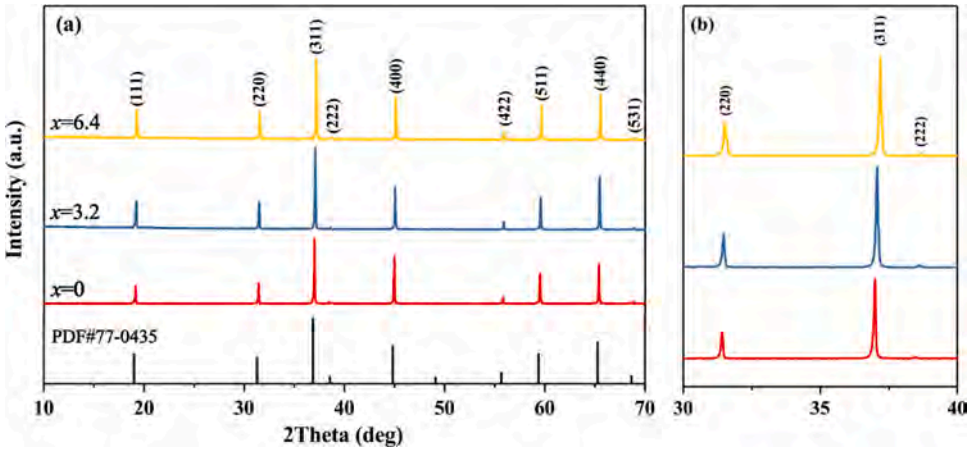

Fig. 1. XRD profiles of $MgAl_2O_4$ + xLiF (x = 0, 3.2, 6.4 mol. %) ceramics sintered at 1575 ℃.

Table 1
FWHM of (311) plane and degree of inversion λ of $MgAl_2O_4$ + xLiF (x = 0, 3.2, 6.4 mol. %) ceramics.

Sample	Sintering temperature (℃)	FWHM(°)	Degree of inversion λ
$MgAl_2O_4$	1575	0.153	0.25
$MgAl_2O_4$ + 3.2 mol.% LiF	1575	0.131	0.43
$MgAl_2O_4$ + 6.4 mol.% LiF	1575	0.122	0.45

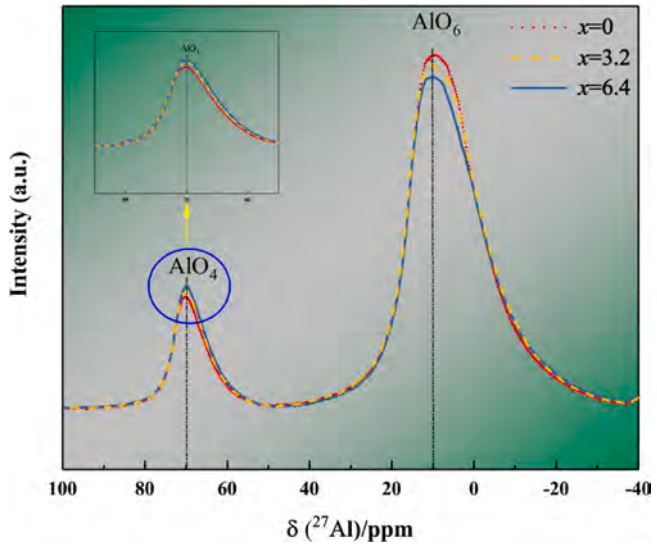

Fig. 2. ^{27}Al NMR spectra of $MgAl_2O_4$ + xLiF(x = 0, 3.2, 6.4 mol. %) ceramics sintered at 1575 ℃.

octahedrally coordinated aluminum. The degree of inversion λ was summarized in Table 1. The λ value of $MgAl_2O_4$ + xLiF (x = 0, 3.2, 6.4 mol. %) ceramics increases with the increase of LiF content, which indicates that the tetrahedral positions in $MgAl_2O_4$ are preferentially occupied by Al^{3+} cations when LiF is doped with $MgAl_2O_4$. The λ value of $MgAl_2O_4$ ceramic sintering at 1575 ℃ is 0.25, which is equivalent to the intermediate configuration of $(Mg_{0.75}Al_{0.25})$ $[Mg_{0.25}Al_{1.75}]$ O_4. The λ value of $MgAl_2O_4$ + 3.2 mol. % LiF ceramic sintering at 1575 ℃ is 0.43, which is equivalent to the intermediate configuration of $(Mg_{0.57}Al_{0.43})$ $[Mg_{0.43}Al_{1.57}]$ O_4. The λ value of $MgAl_2O_4$ + 6.4 mol. % LiF ceramic sintering at 1575 ℃ is 0.45, which is equivalent to the intermediate configuration of $(Mg_{0.55}Al_{0.45})$ $[Mg_{0.45}Al_{1.55}]$ O_4. The schematic diagrams of normal spinel, $(Mg_{0.75}Al_{0.25})$ $[Mg_{0.25}Al_{1.75}]$ O_4, $(Mg_{0.57}Al_{0.43})$ $[Mg_{0.43}Al_{1.57}]$ O_4 and $(Mg_{0.55}Al_{0.45})$ $[Mg_{0.45}Al_{1.55}]$ O_4 viewed along the [100] direction are placed in Fig. 3(a) to (d), respectively.

According to the degree of inversion λ obtained from Eq. (4), the structure information of $MgAl_2O_4$ + xLiF (x = 0, 3.2, 6.4 mol. %) ceramics is obtained through Rietveld refinement [21,22]. The XRD patterns after Rietveld refinement of $MgAl_2O_4$ + xLiF (x = 0, 3.2, 6.4 mol. %) ceramics fired at 1575 ℃ for 8 h are shown in Fig. 4(a)–(c). The specific lattice constant are shown in Fig. 4(d), which decreases with the increase of x value. The refined parameters are listed in Table 2. S. Takahashi et al. considered that the change of MO_4 (M = Mg, Al) volume is the main reason for the variation in the lattice constant of $MgAl_2O_4$ ceramic, which is closely related to the priority sites occupation of Al^{3+} cations [11,17,18]. Table 2 lists the specific volume of MO_4 (M = Mg, Al) tetrahedra in $MgAl_2O_4$ ceramics. The relationship between the volume change of the MO_4 (M = Mg, Al) tetrahedron and the priority sites occupation of Al^{3+} cations can be clarified by estimating the covalency (f_c/s) values of M-O (M = Mg, Al) bonds in the MO_4 tetrahedra. The covalence (f_c) and bond strength (s) of the cation-oxygen bonds can be calculated by Eqs. (5) and (6), respectively [11]:

$$s = (R/R_1)^{-N} \tag{5}$$

$$f_c = as^M \tag{6}$$

Where R_1, N are taken as 1.622, 4.29, respectively [23]; R represents the cation-oxygen bond lengths of MO_4 (M = Mg, Al) tetrahedra in $MgAl_2O_4$ ceramic. Both Al^{3+} and Mg^{2+} have 10 electrons, so the empirical constants M and a are 1.64 and 0.54, respectively [24]. The covalency (f_c/s) values are shown in Fig. 4(d). With the increase of LiF content, the covalencies of M-O bond for the MO_4 (M = Mg, Al) tetrahedra of $MgAl_2O_4$ ceramics increased significantly from 32.8% to 39.7%. From the results, Al^{3+} preferentially occupying the tetrahedral sites increases the covalency of the M-O bond in the MO_4 (M = Mg, Al) tetrahedron, thereby decreasing the lattice constant and the volume of MO_4 tetrahedron.

The relative density is used to evaluate the densification of $MgAl_2O_4$ + xLiF (x = 0, 3.2, 6.4 mol. %) ceramics. The relative densities can be obtained by following equation [25,26]:

$$\rho_{theo} = \frac{A \times Z}{V_{cell} \times N} \tag{7}$$

$$\rho_{relative} = \frac{\rho_{bulk}}{\rho_{theo}} \tag{8}$$

Where V_{cell} is the volume of unit cell (cm^3), N is the Avogadro number (mol^{-1}), Z is the atomic weight (g/mol), and A is the number of atoms in unit cell. The relative densities of $MgAl_2O_4$ + xLiF(x = 0, 3.2, 6.4 mol. %) ceramics sintered at 1575 ℃ for 8 h are listed in Table 2. In all cases, the relative density is greater than 95%, indicating that dense $MgAl_2O_4$ ceramics were synthesized by the solid-state reaction method.

The SEM photographs of the surfaces of $MgAl_2O_4$ + xLiF (x = 0, 3.2, 6.4 mol. %) ceramics fired at 1575 ℃ for 8 h are shown in Fig. 5(a)–(c). The grain sizes of $MgAl_2O_4$ + xLiF (x = 0, 3.2, 6.4 mol. %) ceramics depended on the content of LiF; with increasing LiF content, the grain size of $MgAl_2O_4$ + xLiF (x = 0, 3.2, 6.4 mol. %) ceramics increased from 1.84 to 4.47 μm. This grain growth is related to the rearrangement of Al^{3+} and Mg^{2+} during sintering process. LiF has a low boiling temperature and the addition of LiF will form a transient liquid phase around the spinel phases, thus promoting the rearrangement of Mg^{2+} and Al^{3+} [16]. Therefore, LiF can promote the growth of grains. EDS analysis were performed on spots A and B, and the results are shown in Fig. 6(d) and (e). Molar ratio of Mg:Al in spots A and B is close to 1:2. Both points A and B represent $MgAl_2O_4$, and verify that the grain is $MgAl_2O_4$.

Raman spectra can analyze the lattice vibrations and provides evidence for cation distributions. The Raman spectra of $MgAl_2O_4$ + xLiF (x = 0, 3.2, 6.4 mol. %) ceramics are shown in Fig. 6. $MgAl_2O_4$ possessed 42 normal modes, of which 39 are optical modes and the remaining three are acoustic modes, which can be distributed as the following irreducible representations [8,27,28]:

$$\Gamma = A_{1g}(R) + E_g(R) + 3T_{2g}(R) + 4T_{1u}(IR) + T_{1g} + 2A_{2u} + 2E_u + 2T_{2u} \tag{9}$$

where (IR) represent Infrared-active, (R) represent Raman-active. The spinel structure showed five Raman-active modes. From Fig. 6, five Raman-active modes of $MgAl_2O_4$ were detected, which appear at 311, 407, 670, 727, and 767 cm^{-1} assigned to T_{2g}, E_g, T_{2g}, A_{1g}* and A_{1g} modes, respectively. The Raman band of E_g at 407 cm^{-1} is attributed to the asymmetric bending of the MgO_4 tetrahedron [8]; the Raman

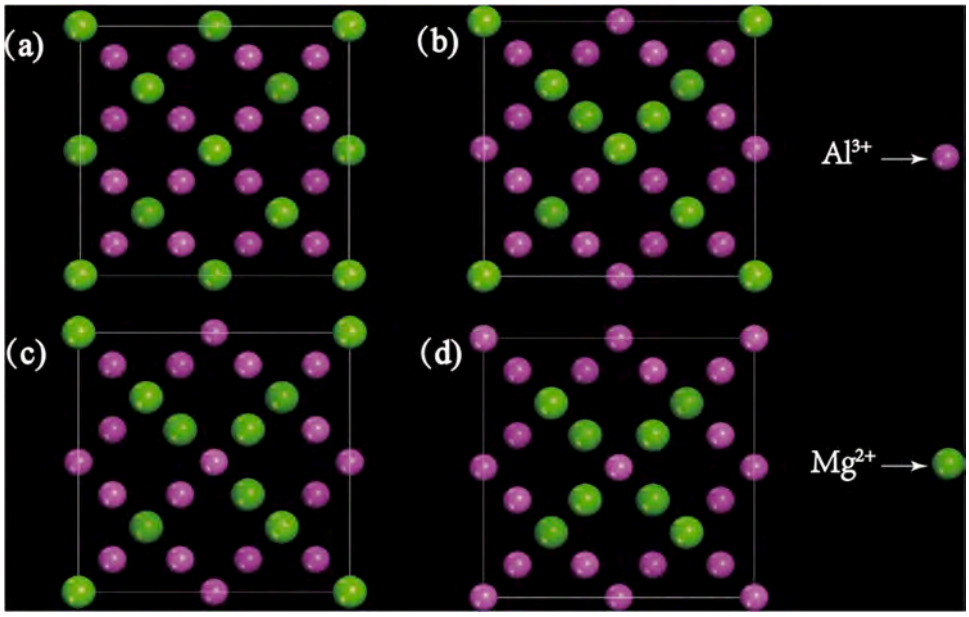

Fig. 3. The schematic diagrams of (a) normal spinel, (b) $(Mg_{0.75}Al_{0.25})[Mg_{0.25}Al_{1.75}]O_4$, (c) $(Mg_{0.57}Al_{0.43})[Mg_{0.43}Al_{1.57}]O_4$ and (d) $(Mg_{0.55}Al_{0.45})[Mg_{0.45}Al_{1.55}]O_4$, viewed along the [100] direction.

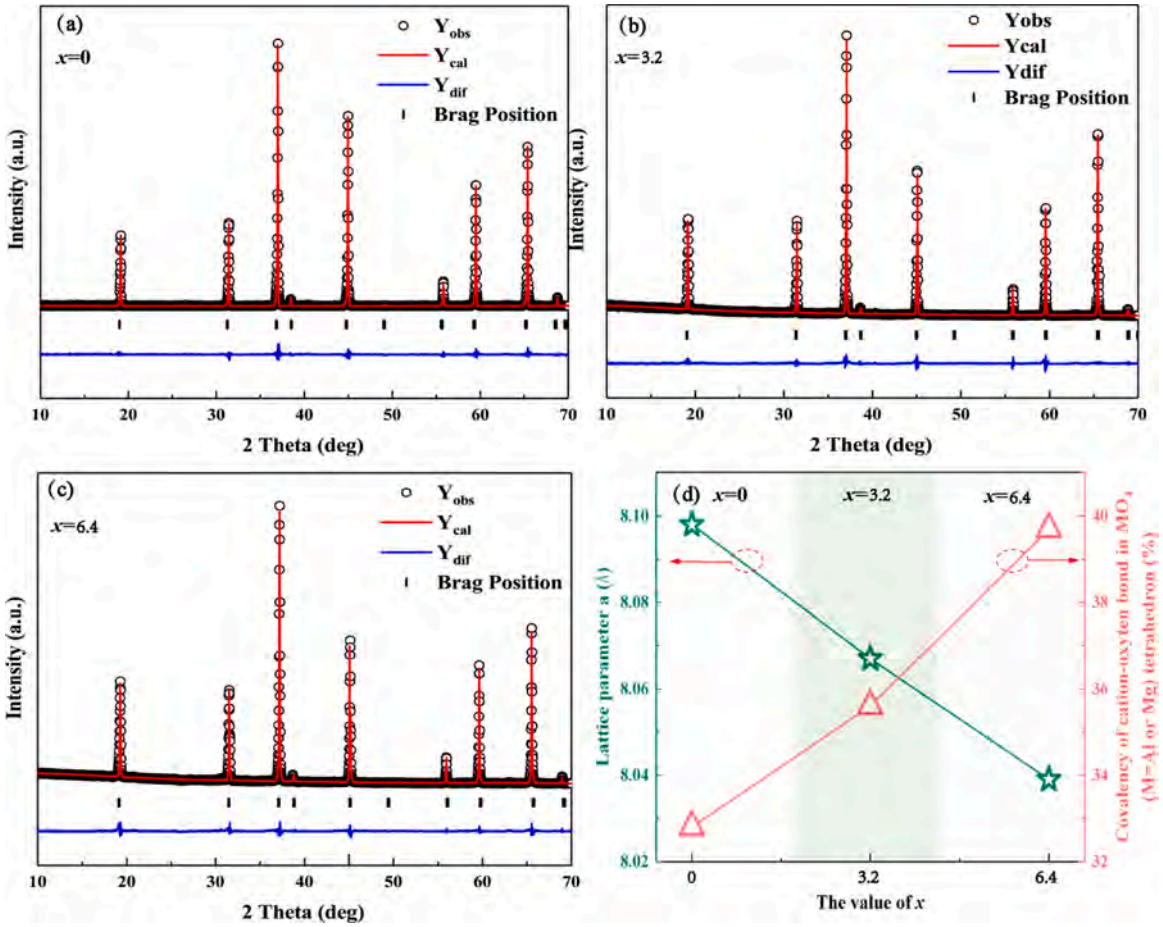

Fig. 4. (a)–(c) The $_{Refined}$ XRD patterns of $MgAl_2O_4 + xLiF$ (x = 0, 3.2, 6.4 mol. %) ceramics sintered at 1575 °C for 8 h; (d) Relationship between lattice parameters, covalency values for the cation-oxygen bonds in the MO_4 (M = Mg, Al) tetrahedra and LiF content.

Table 2
Refined crystal structure parameters, volumes of MO_4 (M = Mg, Al) tetrahedra and relative density of $MgAl_2O_4$ + xLiF (x = 0, 3.2, 6.4 mol. %) ceramics.

Sample	ST (℃)	Atom	Site	Site occupancy	Atomic coordinates			V (Å^3)
					x	y	z	
$MgAl_2O_4$		Mg^{2+}/Al^{3+}	8a	0.75/0.25	0	0	0	
R_{wp} = 3.61, R_p = 2.73	1575 ℃	Mg^{2+}/Al^{3+}	16d	0.12/0.88	0.625	0.625	0.625	3.89
χ^2 = 2.06, $\rho_{relative}$ = 95.3%		O	32e	1	0.3875 (4)	0.3875 (4)	0.3875 (4)	
$MgAl_2O_4$ + 3.2 mol.% LiF		Mg^{2+}/Al^{3+}	8a	0.57/0.43	0	0	0	
R_{wp} = 3.49, R_p = 2.68	1575 ℃	Mg^{2+}/Al^{3+}	16d	0.21/0.79	0.625	0.625	0.625	3.66
χ^2 = 2.09, $\rho_{relative}$ = 95.7%		O	32e	1	0.3854 (5)	0.3854 (5)	0.3854 (5)	
MgAl2O4 + 6.4 mol.% LiF		Mg^{2+}/Al^{3+}	8a	0.55/0.45	0	0	0	
R_{wp} = 3.52, R_p = 2.65	1575 ℃	Mg^{2+}/Al^{3+}	16d	0.22/0.78	0.625	0.625	0.625	3.49
χ^2 = 2.07, $\rho_{relative}$ = 96.2%		O	32e	1	0.3842 (1)	0.3842 (1)	0.3842 (1)	

ST: Sintering temperature; V: Volumes of MO4 tetrahedra.

band of A_{1g} * at 727 cm^{-1} is assigned to the Al-O stretching vibration of AlO_4 tetrahedron. As can be seen in Fig. 6, the intensity of the peak at 407 cm^{-1} decreases with the increase of x value, while the intensity of the peak at 727 cm^{-1} increases with the increase of x value. The result shows that the degree of inversion λ of $MgAl_2O_4$ + xLiF (x = 0, 3.2, 6.4 mol. %) ceramics increases with the increase of LiF content, which is consistent with the ^{27}Al NMR data. The intrinsic properties of ceramic materials are closely related to the damping factor of lattice vibrations. In general, the dielectric loss of ceramic materials increases with the increase in the damping factor. The change of lattice vibration damping factor, which can be judged by the change of FWHM value. Therefore, when the FWHM of the Raman peak changes, the dielectric loss of the ceramic material will also change [29]. As shown in Fig. 6, with the increase of LiF content, the FWHM of Raman at 407 cm^{-1} and 727 cm^{-1} varies greatly. This result shows that the microwave dielectric properties of $MgAl_2O_4$ + xLiF (x = 0, 3.2, 6.4 mol. %) ceramics will change significantly with the increase of LiF content.

The effects of LiF content on the ε_r, $Q\times f$ and TCf values of $MgAl_2O_4$ ceramics are shown in Fig. 7. With increasing the content of LiF, the

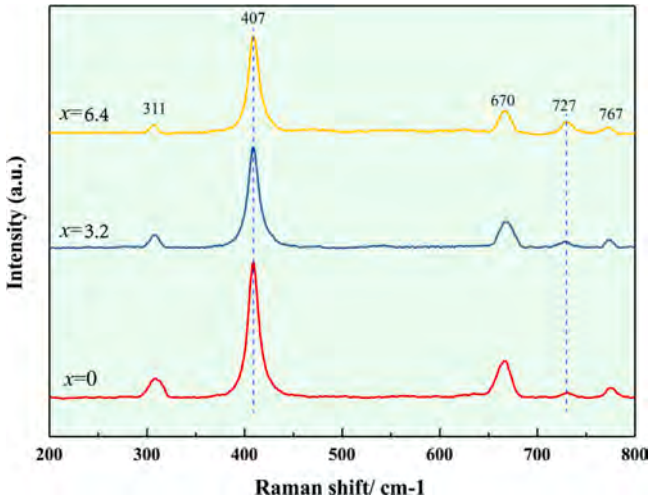

Fig. 6. Raman spectra of $MgAl_2O_4$ + xLiF(x = 0, 3.2, 6.4 mol. %) ceramics sintered at 1575 ℃ for 8 h.

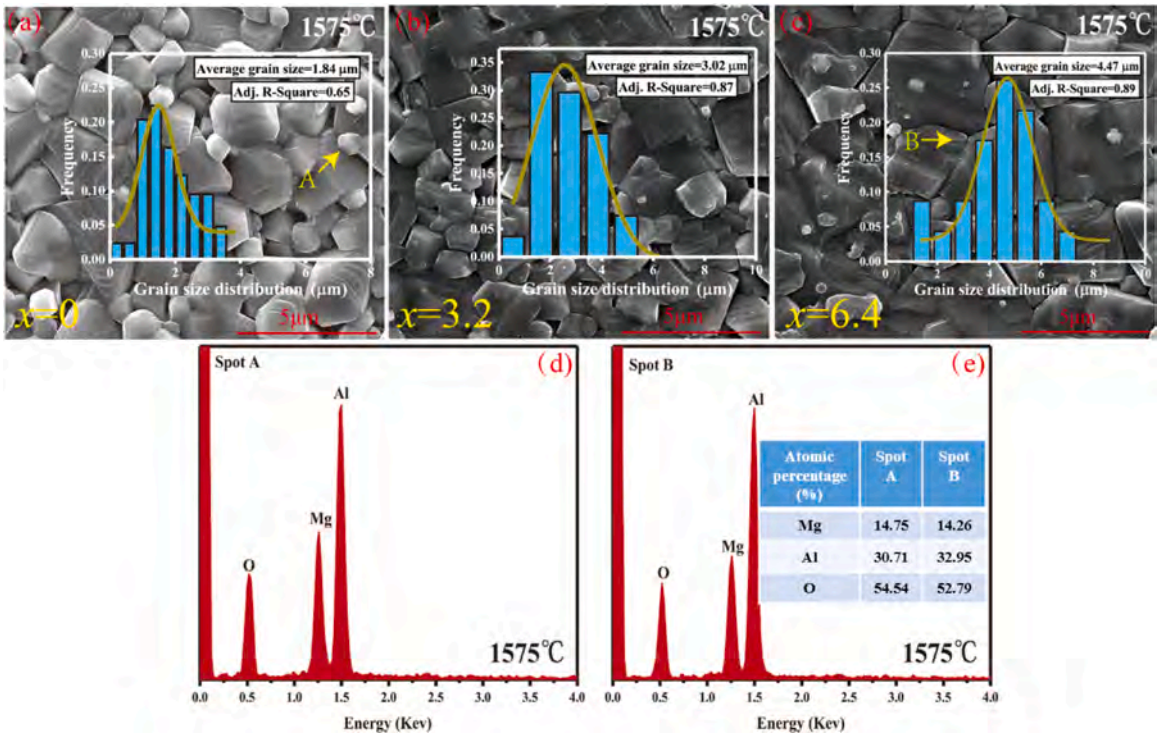

Fig. 5. The SEM micrograph of the $MgAl_2O_4$ + xLiF(x = 0, 3.2, 6.4 mol. %) ceramics sintered at 1575 °C for 8 h: (a) x = 0, (b) x = 3.2, (c) x = 6.4; the EDS analysis of point A and B: (d) point A, (e) point B.

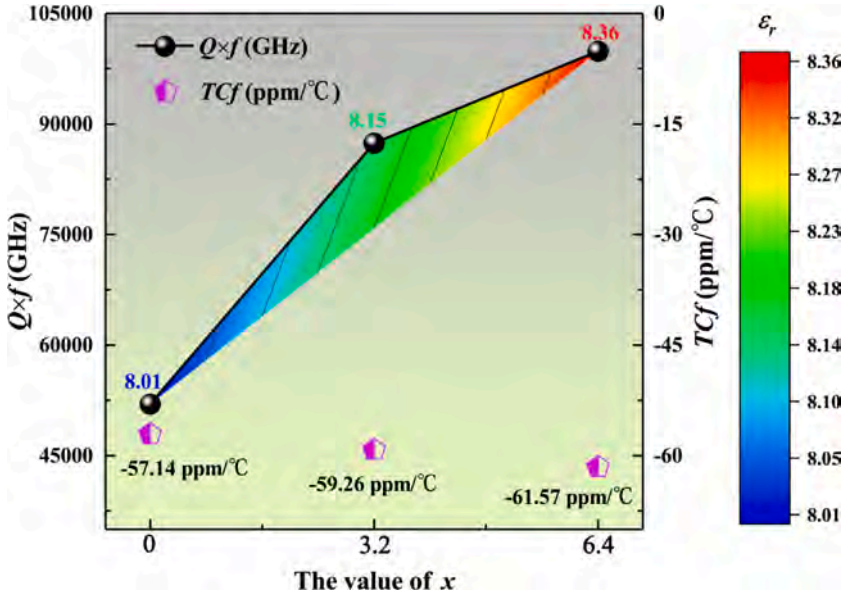

Fig. 7. The dielectric properties of $MgAl_2O_4$ + xLiF (x = 0, 3.2, 6.4 mol. %) ceramics sintered at 1575 °C for 8 h.

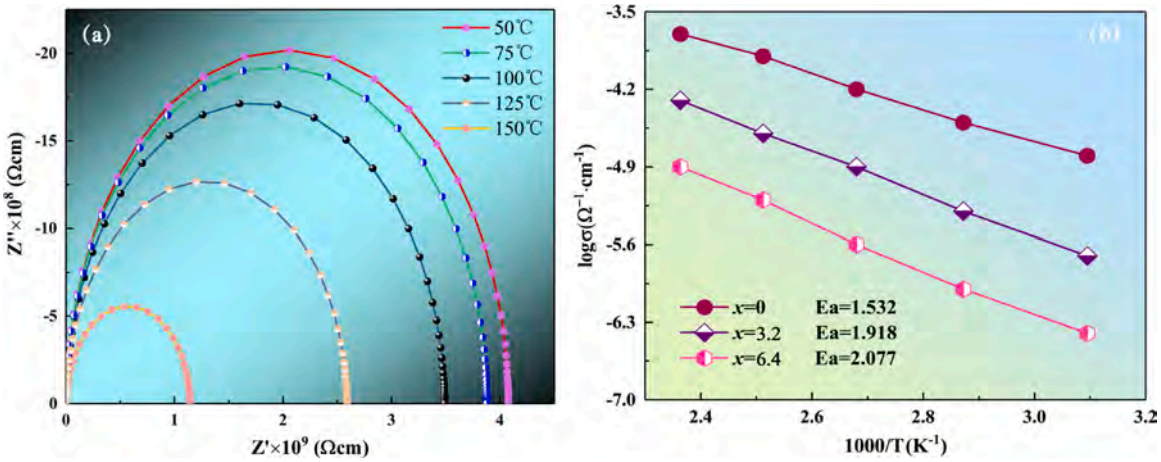

Fig. 8. (a) The impedance spectroscopy diagram of $MgAl_2O_4$ + xLiF(x = 6.4 mol. %) ceramics at different temperatures; (b) Arrhenius fitting plot from the temperature dependence of the bulk conductivity for $MgAl_2O_4$ + xLiF(x = 0, 3.2, 6.4 mol. %) ceramics.

ε_r values of $MgAl_2O_4$ + xLiF (x = 0, 3.2, 6.4 mol. %) ceramics increased from 8.01 to 8.36; the variations in ε_r is consistent with the change of relative density. The $Q\times f$ values of $MgAl_2O_4$ + xLiF (x = 0, 3.2, 6.4 mol. %) ceramics increased from 52,000 GHz to 99,900 GHz with the increase of x value. The $Q\times f$ values of the $MgAl_2O_4$ ceramics is related to its crystallinity, since the FWHM values in (311) plane of the $MgAl_2O_4$ + xLiF (x = 0, 3.2, 6.4 mol. %) ceramics decreased with the increase of LiF content, which indicates that the crystallinity increases with the increase of LiF content, so the $Q\times f$ value also increases. Furthermore, S. Takahashi et al. reported that the difference in the degree of inversion λ of $MgAl_2O_4$ ceramics results in change in the $Q\times f$ value of $MgAl_2O_4$ ceramics, where the larger the λ, the higher the $Q\times f$ values [11,17]. Among the samples prepared in this work, $MgAl_2O_4$ + xLiF (x = 6.4 mol. %) ceramics has the largest λ value, so it has the highest $Q\times f$ value. The impedance spectroscopy diagram of $MgAl_2O_4$ + xLiF (x = 6.4 mol. %) ceramics at different temperatures are shown in Fig. 8(a); the Arrhenius plots of bulk conductivity (σ) for $MgAl_2O_4$ + xLiF (x = 0, 3.2, 6.4 mol. %) ceramics are shown in Fig. 8(b). The activation energy (E_a) obtained from the slope of the fitting line in Fig. 8(b) increased from 1.532 eV to 2.077 eV as the x value increased. Since the approximate value of the intrinsic band gap is $E_g \approx 2E_a$, E_g increases with the increase of x value, which means that the conductivity decreases with the increase of x value [30,31]. Therefore, samples with high x values have better quality factors than samples with low x values, which further confirms the previous conclusion. The TCf values of the $MgAl_2O_4$ + xLiF (x = 0, 3.2, 6.4 mol. %) ceramics ranged from − 57.14 to − 61.57 ppm/℃ and changed little. The TCf value of $MgAl_2O_4$ is − 57.14 ppm/℃, and the TCf value of LiF is − 120 ppm/℃. According to the mixture rules: $TCf = V_1TCf_1 + V_2TCf_2$, where V represents the volume fraction. The addition of LiF will significantly increase the TCf value of $MgAl_2O_4$ ceramics in the negative direction. The experimental results show that the TCf value of $MgAl_2O_4$ ceramic has little change, because LiF diffused out of the spinel lattice during the sintering process.

4. Conclusions

$MgAl_2O_4$ + xLiF (x = 0, 3.2, 6.4 mol. %) ceramics were synthesized by solid-state reaction method. The cation distribution was systematically investigated by ^{27}Al NMR and Raman spectra. The results showed that Al^{3+} in the spinel structure will preferentially occupy tetrahedral sites with the increase of x value, and the λ values of the $MgAl_2O_4$ + xLiF (x = 0, 3.2, 6.4 mol. %) ceramics sintered at 1575 ℃ increases from 0.25 to 0.45. The covalency (f_c/s) values of M-O

(M = Mg, Al) bonds in the MO_4 tetrahedra of $MgAl_2O_4$ + xLiF (x = 0, 3.2, 6.4 mol. %) ceramics gradually increased, from 32.8% to 39.7%. The grain size of $MgAl_2O_4$ + xLiF (x = 0, 3.2, 6.4 mol. %) ceramics increased from 1.84 to 4.47 μm with the increase of LiF content. The variations in ε_r is consistent with the change of relative density. The $Q\times f$ value of $MgAl_2O_4$ ceramics is significantly affected by the degree of inversion λ of $MgAl_2O_4$ ceramics. The TCf values of the samples changed little. Pure $MgAl_2O_4$ ceramics have the overall performance when sintered at 1575 °C for 8 h: ε_r = 8.01, $Q\times f$ = 52,000 GHz, TCf = − 57.14 ppm/°C. With 6.4 mol. % LiF added, excellent microwave dielectric properties were achieved at 1575 °C for 8 h: ε_r = 8.36, $Q\times f$ = 99,900 GHz, TCf = − 61.57 ppm/°C.

CRediT authorship contribution statement

Qin Tianying: Conceptualization, Methodology, Software, Validation, Formal analysis, Investigation, Writing – original draft, Writing – review & editing. **Zhong Chaowei:** Conceptualization, Methodology, Supervision, Project administration, Funding acquisition, Writing – review & editing. **Shang Yong:** Methodology, Validation, Data curation, Writing – review & editing. **Cao Lei:** Software, Validation, Formal analysis, Investigation. **Wang Mingxia:** Formal analysis, Investigation. **Tang Bin:** Supervision, Project administration, Funding acquisition, Writing – review & editing. **Zhang Shuren:** Supervision, Project administration, Funding acquisition, Writing – review & editing.

Declaration of Competing Interest

The authors declare that they have no known competing financial interests or personal relationships that could have appeared to influence the work reported in this paper.

Acknowledgments

This work was all funded by the National Natural Science Foundation of China (No. 51672038), and the authors are very grateful.

References

[1] L. Pang, D. Zhou, Z. Qi, W. Liu, Z. Yue, I. Reaney, Structure–property relationships of low sintering temperature scheelite-structured (1−x) $BiVO_4$–$x$$LaNbO_4$ microwave dielectric ceramics, J. Mater. Chem. C 5 (10) (2017) 2695–2701.
[2] H. Li, P. Zhang, S. Yu, H. Yang, B. Tang, F. Li, S. Zhang, Structural dependence of microwave dielectric properties of spinel structured $Mg_2(Ti_{1-x}Sn_x)O_4$ solid solutions: crystal structure refinement, Raman spectra study and complex chemical bond theory, Ceram. Int. 45 (9) (2019) 11639–11647.
[3] I. Kagomiya, Y. Matsuda, K. Kakimoto, H. Ohsato, Microwave dielectric properties of YAG ceramics, Ferroelectrics 387 (1) (2019) 1–6.
[4] T. Qin, C. Zhong, H. Yang, Y. Qin, S. Zhang, Investigation on glass-forming ability, flexural strength and microwave dielectric properties of Al_2O_3-doped LMZBS glasses, Ceram. Int. 45 (8) (2019) 10899–10906.
[5] Z. Fang, B. Tang, F. Si, S. Zhang, Temperature stable and high-Q microwave dielectric ceramics in the $Li_2Mg_{3-x}Ca_xTiO_6$ system (x=0.00–0.18), Ceram. Int. 43 (2) (2017) 1682–1687.
[6] K. Surendran, P. Bijumon, P. Mohanan, M. Sebastian, (1-x)$MgAl_2O_4$-$x$$TiO_2$ dielectrics for microwave and millimeter wave applications, Appl. Phys. A 81 (4) (2005) 823–826.
[7] M. O'horo, A. Frisillo, W. White, Lattice vibrations of $MgAl_2O_4$ spinel, J. Phys. Chem. Solids 34 (1974) 23–28.
[8] H. Cynn, S. Sharma, T. Cooney, M. Nicol, High-temperature Raman investigation of order-disorder behavior in the $MgAl_2O_4$ spinel, Phys. Rev. B Condens. Matter 45 (1) (1992) 500–502.
[9] S. Slotznick, S. Shim, In situ Raman spectroscopy measurements of $MgAl_2O_4$ spinel up to 1400°C, Am. Mineral. 93 (2–3) (2008) 470–476.
[10] E. Blaakmeer, F. Rosciano, E. Eck, Lithium doping of $MgAl_2O_4$ and $ZnAl_2O_4$ investigated by high-resolution solid state NMR, J. Phys. Chem. C 119 (14) (2015) 7565–7577.
[11] T. Takahashi, A. Kan, H. Ogawa, Microwave dielectric properties and crystal structures of spinel-structured $MgAl_2O_4$ ceramics synthesized by a molten-salt method, J. Eur. Ceram. Soc. 37 (3) (2017) 1001–1006.
[12] K. Rozenburg, I. Reimanis, H. Kleebe, R. Cook, Sintering kinetics of a $MgAl_2O_4$spinel doped with LiF, J. Am. Ceram. Soc. 91 (2) (2008) 444–450.
[13] K. Rozenburg, I. Reimanis, H. Kleebe, R. Cook, Chemical interaction between LiF and $MgAl_2O_4$ spinel during sintering, J. Am. Ceram. Soc. 90 (7) (2007) 2038–2042.
[14] W. Luo, R. Xie, M. Ivanov, Y. Pan, H. Kou, J. Li, Effects of LiF on the microstructure and optical properties of hot-pressed $MgAl_2O_4$ ceramics, Ceram. Int. 43 (9) (2017) 6891–6897.
[15] M. Müller, H. Kleebe, H. Chan, Sintering mechanisms of LiF-doped Mg-Al-spinel, J. Am. Ceram. Soc. 95 (10) (2012) 3022–3024.
[16] I. Reimains, H. Kleebe, Reactions in the sintering of $MgAl_2O_4$ spinel doped with LiF, Int. J. Mater. Res. 98 (12) (2007) 1273–1278.
[17] S. Takahashi, H. Ogawa, A. Kan, Electronic states and cation distributions of $MgAl_2O_4$ and $Mg_{0.4}Al_{2.4}O_4$ microwave dielectric ceramics, J. Eur. Ceram. Soc. 38 (2) (2018) 593–598.
[18] S. Takahashi, A. Kan, H. Ogawa, Effects of cation distribution on microwave dielectric properties of Mg_{1-x} $Zn_xAl_2O_4$ ceramics, Mater. Chem. Phys. 200 (2017) 257–263.
[19] V. Sepelak, S. Indris, I. Bergmann, A. Feldhoff, K. Becker, P. Heitjans, Nonequilibrium cation distribution in nanocrystalline $MgAl_2O_4$ spinel studied by ^{27}Al magic-angle spinning NMR, Solid State Ion. 177 (26–32) (2006) 2487–2490.
[20] S. Takahashi, A. Kan, H. Ogawa, Microwave dielectric properties and crystal structures of $Mg_{0.7}Al_{2.2}O_4$ and $Mg_{0.4}Al_{2.4}O_4$ ceramics with defect structures, J. Am. Ceram. Soc. 100 (8) (2017) 3497–3504.
[21] T. Qin, C. Zhong, Y. Qin, B. Tang, S. Zhang, The structure evolution and microwave dielectric properties of $MgAl_{2-x}(Mg_{0.5}Ti_{0.5})_xO_4$ solid solutions, Ceram. Int. 46 (11) (2020) 19046–19051.
[22] Y. Lai, H. Su, G. Wang, X. Tang, X. Huang, X. Liang, et al., Low-temperature sintering of microwave ceramics with high Qf values through LiF addition, J. Am. Ceram. Soc. 102 (4) (2018) 1893–1903.
[23] I. Brown, K. Wu, Empirical parameters for calculating cation-oxygen bond valences, Acta Crystallogr. Sect. B 32 (7) (1976) 1957–1959.
[24] I. Brown, R. Shannon, Empirical bond-strength-bond-length curves for oxides, Acta Crystallogr. Sect. A 29 (3) (1973) 266–282.
[25] B. Tang, Q. Xiang, Z. Fang, X. Zhang, Z. Xiong, H. Li, C. Yuan, S. Zhang, Influence of Cr^{3+} substitution for Mg^{2+} on the crystal structure and microwave dielectric properties of $CaMg_{1-x}Cr_{2x/3}Si_2O_6$ ceramics, Ceram. Int. 45 (9) (2019) 11484–11490.
[26] T. Qin, C. Zhong, Y. Qin, B. Tang, S. Zhang, Low-temperature sintering mechanism and microwave dielectric properties of $ZnAl_2O_4$-LMZBS composites, J. Alloy. Compd. 797 (2019) 744–753.
[27] A. Chopelas, A. Hofmeister, Vibrational spectroscopy of aluminate spinels at 1 atm and of MgAl2O4 to over 200 kbar, Phys. Chem. Miner. 18 (1991) 279–293.
[28] V. D'Ippolito, G. Andreozzi, D. Bersani, P. Lottici, Raman fingerprint of chromate, aluminate and ferrite spinels, J. Raman Spectrosc. 46 (12) (2015) 1255–1264.
[29] X. Sun, Z.W. Lin, X.X. Hu, W.M. Yao, B. Bai, H.Y. Wang, D.Y. Li, Z. Chen, H. Cheng, W.G. Pan, M.G. Deng, G.J. Xu, H.P. Tu, J.W. Chen, Q.W. Deng, Z.J. Yu, J.X. Zheng, Biofilm formation in erythromycin-resistant Staphylococcus aureus and the relationship with antimicrobial susceptibility and molecular characteristics, Microb. Pathog. 124 (4) (2018) 47–53.
[30] X.K. Lan, J. Li, Z.Y. Zou, M.Q. Xie, G.F. Fan, W.Z. Lu, W. Lei, Improved sinterability and microwave dielectric properties of $[Zn_{0.5}Ti_{0.5}]^{3+}$-doped $ZnAl_2O_4$ spinel solid solution, J. Am. Ceram. Soc. 102 (10) (2019) 5952–5957.
[31] J. Zang, M. Li, D.C. Sinclair, T. Frömling, W. Jo, J. Rödel, Impedance spectroscopy of $(Bi_{1/2}Na_{1/2})TiO_3$-$BaTiO_3$ based high-temperature dielectrics, J. Am. Ceram. Soc. 97 (9) (2014) 2825–2831.